Investigation of self-organized criticality behavior of edge plasma transport in Torus experiment of technology oriented research

Y. H. Xu, S. Jachmich, and R. R. Weynants
Laboratory for Plasma Physics, Ecole Royale Militaire/Koninklijke Militaire School, Euratom-Belgian State Association, Avenue de la Renaissance 30, B-1000 Brussels, Belgium[a)]

A. Huber, B. Unterberg, and U. Samm
Institute für plasmaphysik, Forschungzentrum Jülich GmbH, D-52425 Jülich, Germany[a)]

(Received 1 April 2004; accepted 2 September 2004; published online 29 October 2004)

The self-organized criticality (SOC) behavior of the edge plasma transport has been studied using fluctuation data measured in the plasma edge and the scrape-off layer of Torus experiment of technology oriented research tokamak [H. Soltwisch *et al.*, Plasma Phys. Controlled Fusion **26**, 23 (1984)] before and during the edge biasing experiments. In the "nonshear" discharge phase before biasing, the fluctuation data clearly show some of the characteristics associated with SOC, including similar frequency spectra to those obtained in "sandpile" transport and other SOC systems, slowly decaying long tails in the autocorrelation function, values of Hurst parameters larger than 0.5 at all the detected radial locations, and a radial propagation of avalanchelike events in the edge plasma area. During the edge biasing phase, with the generation of an edge radial electric field E_r and thus of $E_r \times B$ flow shear, contrary to theoretical expectation, the Hurst parameters are substantially enhanced in the negative flow shear region and in the scrape-off layer as well. Concomitantly, it is found that the local turbulence is well decorrelated by the $E_r \times B$ velocity shear, consistent with theoretical predictions. © *2004 American Institute of Physics*. [DOI: 10.1063/1.1810160]

I. INTRODUCTION

Understanding the nature of anomalous transport in magnetically confined plasmas is still a subject of intensive research. It is known that such cross-field transport can be caused by several distinct mechanisms such as *diffusion* by random Coulomb collisions or turbulence mixing, *convection* by convective cells, avalanches or magnetic stochasticity, and *relaxation oscillations* by sawteeth or edge localized modes, etc. A purely diffusive model proposed earlier by Kadomtsev leads to a gyro-Bohm scaling of heat diffusivity,[1] while the experimental results revealed that the scaling may vary between gyro-Bohm and Bohm.[2,3] The essential difference between these two scalings is the characteristic dimension of the transport, which in the latter case is on the order of the system size and in the former on the order of the correlation length of the turbulence. Long-range spatial and temporal correlation through scale invariance is the central idea of the concept of self-organized criticality (SOC),[4–7] in which avalanche-type long-range transport is the result of the self-organization of near-critical, nonlinear dynamical systems. In general, mixed diffusive and SOC dynamics will control transport. Distinguishing the SOC channel from the diffusive one can be done by the experimental identification of a number of features considered as key ingredients of SOC behavior,[5,7–10] such as (i) the existence of a critical threshold, (ii) radial correlations in fluctuations over distances longer than turbulence correlation lengths, (iii) time correlations on the order of many times the turbulence decorrelation time, (iv) the existence of f^{-1} behavior in the measured broadband fluctuation spectrum as an indication of important degree of avalanche overlapping, (v) the observation of self-similarity. In recent years, experimental evidence of these and other features, such as long-range time correlations (or self-similarity),[11] empirical similarity of frequency spectra,[12] intermittent behavior,[13] radial propagation of avalanchelike events,[14] and the self-similar distortion of Poisson-distributed quiet times to the power-law form[15] of plasma fluctuations has been found in several fusion devices consistent with some SOC predictions, although other non-SOC explanations of long-range correlation and bursty transport are possible.[16] Nevertheless, on the other hand, absence of long-range correlation has also been reported from both "nonfusion" plasmas[17] and more recently the ADITYA tokamak.[18]

In this paper, we report on the analysis of fluctuation data measured in the plasma edge and the scrape-off layer (SOL) of the TEXTOR (Torus experiment of technology oriented research) tokamak in the edge electrode biasing experiment.[19,20] A partial account of this work was published earlier.[21] Two goals were aimed at. First, we look for possible evidence of SOC behavior in the ohmically heated plasmas in TEXTOR before biasing. This discharge phase is slightly different from the "standard" ohmic discharge in TEXTOR. Because of the insertion of the electrode at zero voltage, the E_r profile in the plasma boundary is flattened with approximately zero $E_r \times B$ shear rate, while in the "standard" ohmic discharge a naturally occurring $E_r \times B$ velocity shear layer often exists around the last closed flux surface (LCFS). We will further on refer to this phase as the "nonshear" phase. Second, we investigate how long and short time transport events are affected by a controlled sheared

[a)]Partner in the Trilateral Euregio Cluster.

edge $E_r \times B$ flow as imposed by edge electrode polarization during the biasing or "shear" phase. For this, we systematically studied the power spectra $S(f)$, autocorrelation functions (ACF), and the Hurst parameters via rescaled range (R/S) analysis[22,23] and structure functions (SFs) analysis[24–26] of the potential fluctuation data detected at different radial locations. The rest of the paper is organized as follows. Section II gives description of the experimental setup. The results and discussions are presented in Sec. III and conclusions formulated in Sec. IV. A concise definition of some of the statistical tools is given in the Appendix.

II. EXPERIMENTAL CONDITIONS

The experiments subjected to this study were performed in the TEXTOR tokamak with the following discharge parameters: $R=175$ cm, $a\cong 48$ cm, $B_T=2.33$ T, $I_p=200$ kA, $V_l=1$ V, and $\overline{n_e}=1.0\times 10^{19}$ m^{-3} in ohmically heated plasmas. The floating potential fluctuations were measured in both the plasma edge and the SOL region by a set of Langmuir probes consisting of carbon tips with 3.5 mm in diameter. The probe pins are 3.75 mm separated radially. The whole probe system can be moved radially from shot to shot. But during each shot, the radial positions for all probe pins are fixed. The fluctuation data were digitized at a rate of 500 kHz. For creating an edge electric field E_r and hence a sheared $E_r \times B$ flow, a biasing voltage quickly ramped from 0 to 600–700 V was applied between an inserted electrode located at $r\cong 41$ cm and the toroidal belt limiter (ALT-II) during the flat top of the discharge. The time evolution of a typical set of discharge parameters of the edge electrode biasing experiment is displayed in Fig. 1. From Fig. 1(a), we can see that in the "nonshear" phase before biasing, the discharge wave forms of the plasma current $I_p(\sim 200$ kA), central line-averaged electron density $\overline{n_{e0}}(\sim 1.0\times 10^{19}$ m$^{-3})$, and loop voltage $V_i(\sim 1$ V) all keep rather flat. Shown in Fig. 1(b) are the voltage (V_{bia}, thin line) and current (I_{bia}, thick line) signals on the polarized electrode. The figure shows that before biasing, V_{bia} is set to be zero (as stated earlier) and a current of $I_{\mathrm{bia}}\approx 20$ A is drawn by the electrode due to its insertion into the plasma. At about 1.05 s, a positive biasing voltage is applied to the electrode, starting as a quick linear ramp and then holding constant at $V_{\mathrm{bia}}\cong 600$ V in an averaged sense. As explained previously,[20] the slow oscillation of V_{bia} at a frequency of $f\approx 25$ Hz is caused by the ringing of the voltage power supply upon changes in its plasma load during the period of E_r bifurcation. The effects of this low-frequency oscillation on the fluctuation data measured by the probes have been filtered. From 1.05 s, I_{bia} increases linearly until the E_r bifurcation occurs at about 1.2 s resulting in a drop in I_{bia}. The discharge then evolves into another quasi-stationary state phase. The influence of biasing on edge potential fluctuations can be seen in Figs. 1(c) and 1(d) , where time traces of the floating potential measured at two radial positions ($r=47.6$ cm inside the LCFS and $r=49.5$ cm in the SOL) are displayed. Here, we can see that after the polarization, the potential fluctuation amplitudes are clearly increased in the plasma edge and decreased in the SOL, respectively.

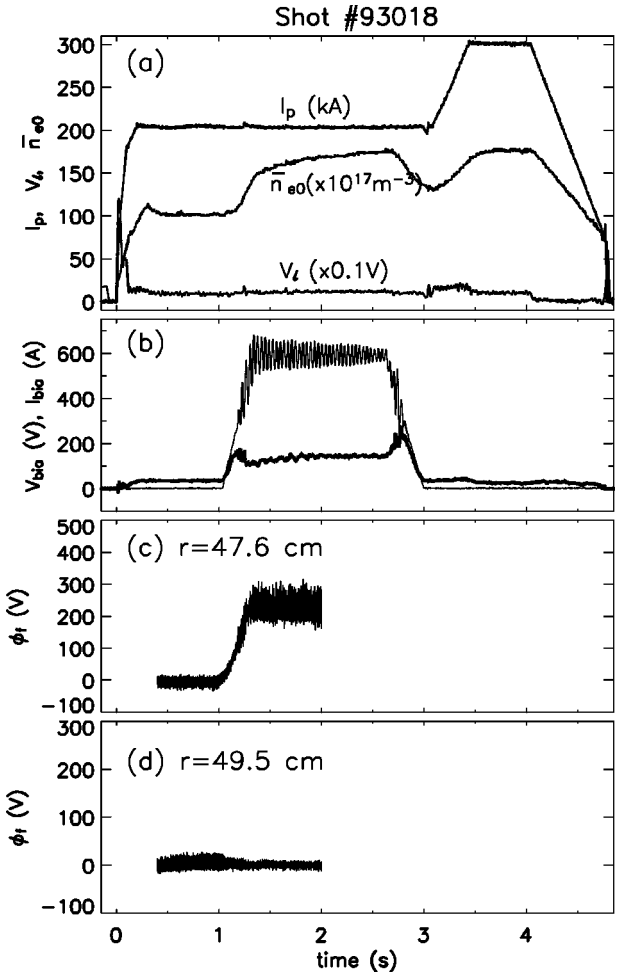

FIG. 1. Time evolution of discharge parameters in the edge electrode biasing experiment on TEXTOR (shot No. 93 018). (a) Plasma current, line-averaged electron density, and loop voltage, (b) voltage (thin line) and current (thick line) signals on the polarized electrode. Shown in (c) and (d) are time traces of floating potential measured at $r=47.6$ cm and $r=49.5$ cm, respectively.

Typical radial dependences of the floating potential ϕ_f detected by probes before (~ 0.6 s) and during (~ 1.6 s) the polarization of another similar shot are plotted in Fig. 2 along with the profiles of the radial electric field E_r and E_r shear. Here, E_r is estimated directly from the radial derivative of ϕ_f neglecting the contribution from the T_e gradient, and therefore underestimating E_r slightly. The radial derivations for calculating E_r and E_r shear are taken by differentiating spline fits and smoothing extraneous curvature before taking next derivative. From the figures, it can be seen that in the "nonshear" phase before biasing, the potential profile, across the whole measured plasma edge and SOL region, is very flat, resulting in rather flat E_r and E_r shear profiles. The values of ϕ_f, E_r, and E_r shear are all close to zero in that phase. Therefore, the poloidal plasma rotation caused by $E_r \times B$ drift in that stage is also very small. This may provide advantages for the study of the SOC behavior because in such "quiet" plasmas the possible influence due to correlated blobs moving in the poloidal direction on the long-range correlations can be excluded. During the polarized phase, the ϕ_f profile is highly enhanced inside the LCFS, leading to a

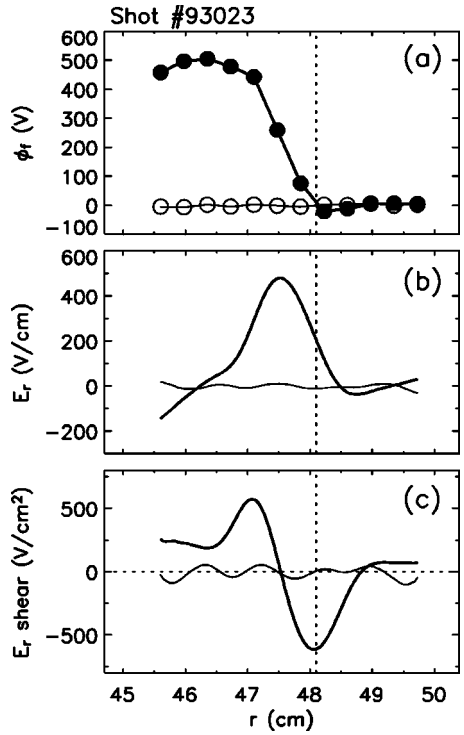

FIG. 2. Radial profiles of (a) the floating potential ϕ_f, (b) the radial electric field E_r, and (c) the E_r shear before (~0.6 s, open symbols and thin lines) and during (~1.6 s, filled symbols and thick lines) the polarization. The symbols in (a) indicate the locations of probe pin measurements. The vertical dotted line marks the approximate position of the last closed flux surface.

narrow positive E_r structure between $r \approx 46.7$ cm and $r \approx 48.3$ cm, with a maximal value ~480 V cm, as shown in Fig. 2(b). The resultant E_r shear is positive in the plasma edge (maximal ~600 V/cm^2) and negative across the LCFS location (~−600 V/cm^2), respectively [see Fig. 2(c)].

III. RESULTS AND DISCUSSIONS

A. Frequency spectra, autocorrelation functions, and Hurst parameters in the "nonshear" discharge phase

The first aim is to investigate the existence of SOC characteristics in the "nonshear" discharge phase. For this, we mainly studied some typical features associated with SOC dynamics in the fluctuation data, i.e., autopower frequency spectrum, ACF, and the Hurst parameter of the fluctuations. A concise definition of these notions is given in the Appendix.

In the present study of long-range correlations, a practical importance is that the data samples used should be stationary. We therefore start with a test of the stationarity of the floating potential fluctuation data record using Eqs. (3) and (4) of the SFs analysis exposed in the Appendix. The results are shown in Fig. 3 as examples for two radial locations (one at $r=47.1$ cm in the plasma edge and the other at $r=49.4$ cm in the SOL) before and during the biasing, respectively. In Fig. 3, for each case, the qth order SFs of the raw data $X(t)$, $S_{x,q}(\tau)$, is plotted vs τ for $q=0.5,1,2,3,4,5$. It can be seen that, in each log-log plot, there always exists a certain range of τ, from about 100–150 μs (marked by vertical dotted lines) to $\geqslant$3000 μs, where $S_{x,q}(\tau)$ is roughly constant with zero slope, indicating that the data are stationary within these ranges. Furthermore, the corresponding SFs of the integrated data $S_{w,q}(\tau)$ in these ranges can be then applied to determine the Hurst exponents.

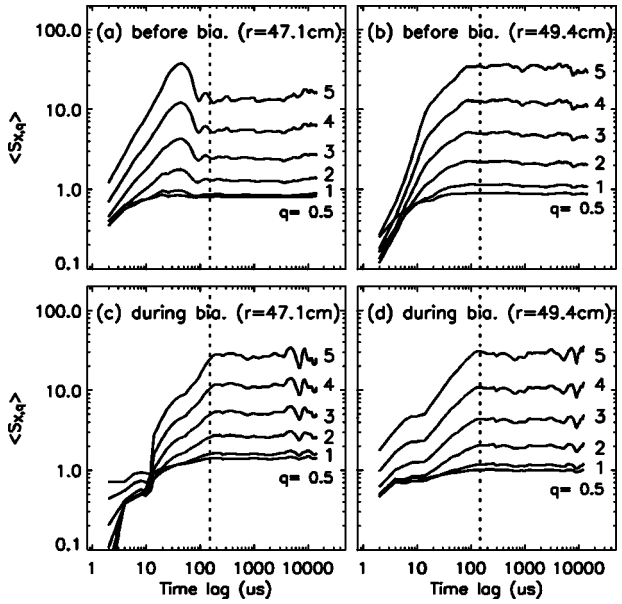

FIG. 3. Structure function $S_{x,q}(\tau)$ for $q=0.5$, 1, 2, 3, 4, 5, of the floating potential fluctuation data detected at (a) $r=47.1$ cm before biasing; (b) $r=49.4$ cm before biasing; (c) $r=47.1$ cm during biasing; and (d) $r=49.4$ cm during biasing. Data are stationary for time lag from about 100–150 μs (marked by vertical dotted lines) to $\geqslant$3000 μs.

Detailed measurements, presented in Fig. 4, were done at three different radial positions: (i) $r=50.1$ cm in the SOL; (ii) $r=48.1$ cm around the LCFS, and (iii) $r=45.6$ cm in the edge plasma zone. For the present analysis, the data set of each discharge was broken into eight unoverlapping sub blocks of 8000 points (total time lag=16 ms). The $S(f)$, ACF, R/S [as defined in Eq. (2) of the Appendix] and SF [the average of the $1/q$ power of $S_{w,q}(\tau)$, $\langle S_{w,q}^{1/q} \rangle$, as defined in Eq. (5) of the Appendix], for each sub block was calculated for the floating potential fluctuation data and then averaged over the eight sub blocks.

In Figs. 4(a) and 4(d), it can be seen that either in the SOL or nearby the LCFS, the frequency spectrum $S(f)$ shows roughly three distinct regions in the frequency range of $f=(0.2-250)$ kHz with approximate decay indices of 0, −1, and −2, respectively, although the separation between ranges is not sharp. These results are in good agreement with other experimental observations[12,27–29] and resemble those obtained in the sandpile modeling and in turbulence model realizations of SOC systems,[5,9,30] i.e., (i) a high-frequency part (scaled as f^{-n}, where n is 2 or higher) signifying small scale events involving very small parts of the system, (ii) a low-frequency part (scaled nearly as f^0) reflecting single events with a global scale, and (iii) the intermediate range (with f^{-1} dependence), which has been related to the overlapping of avalanche transport. Figures 4(a) and 4(d) also show that the frequency range of each subregion is slightly different. These differences might be associated with local variations in the

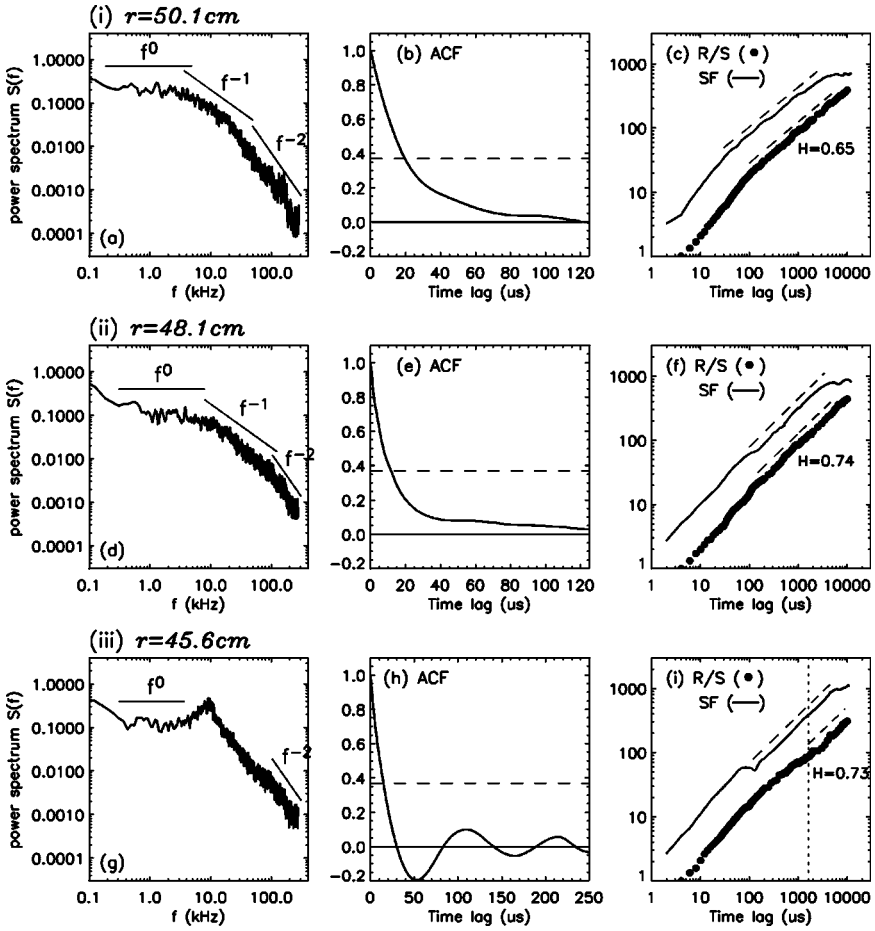

FIG. 4. Power spectrum $S(f)$ [(a), (d), (g)], autocorrelation function (ACF) [(b), (e), (h)] and R/S (SF) analysis [(c), (f), (i)] of the floating potential fluctuations measured at three radial positions: (i) $r=50.1$ cm in the SOL, (ii) $r=48.1$ cm nearby the LCFS, and (iii) $r=45.6$ cm in the plasma edge in the "nonshear" discharge phase before biasing. In (c), (f), and (i), R/S values are shown by solid circles; the SF curve in each plot is the average of the $1/q$ power of $S_{w,q}(\tau)$ for $q=0.5$, 1, 2, 3, 4, 5. The dashed lines in (c), (f), and (i) are the best fit to the R/S slope with $H=0.65$, 0.74, and 0.73, respectively; and the parallel ones show comparison with the SF curves.

importance of diffusive versus SOC transport.[10] It is interesting to see that from the SOL to the LCFS zone, the intermediate f^{-1} range, shifting from (3–20) to (8–100) kHz, becomes broader, implying that the nonlinear interaction of transport events is stronger in the vicinity of the LCFS than in the SOL. In the plasma edge, Fig. 4(g) displays strong coherent modes (CMs) in the power spectrum with peaks at about 10 kHz. This can also be seen in Fig. 3(a) at another edge position, where $S_{x,q}(\tau)$ shows periodic oscillations in its first several harmonics. It has been found that this CM harmonic $S(f)$ usually appears at locations starting from ~10 mm inside the limiter. As seen in the figure, these coherent modes hide the intermediate f^{-1} range arising from the background turbulence, but the other two frequency regions remain similar to those observed at other two radial positions.

The corresponding ACFs measured at the above three positions are shown in Figs. 4(b), 4(e), and 4(h), respectively. From the figures, it can be seen that at the small time lags the value of ACF at each position drops very rapidly with time. The peak part of the ACF carries information on the correlation of local fluctuations. Here, the e-folding time of the ACF, i.e., the width of the peak τ_D is taken to be the decorrelation time of the local turbulence.[31] Figures 4(b), 4(e), and 4(h) show that τ_D is around 10–20 μs at the three measured locations (see dashed lines). The existence of long-time correlation should be evident from an algebraic tail in the ACF.[32] Such a slow decay can be clearly seen in Figs. 4(b) and 4(e), over large intervals of time lags until $\tau \geqslant 120$ μs. Because of 10 kHz CM harmonics, the ACF tail measured at the plasma edge ($r=45.6$ cm) strongly oscillates at a main CM period of ~100 μs, as displayed in Fig. 4(h).

Self-similarity is studied by means of the Hurst parameter H, using the R/S and SF methods for cross checking the accuracy of H value obtained. The corresponding plots of R/S values (solid circles) versus time lags at the above three radial positions are shown in Figs. 4(c), 4(f), and 4(i), respectively. From Figs. 4(c) and 4(f), we can see that for time lags smaller than a few $\tau_D(\tau<100$ μs), there is a transient process giving a constant slope of about 0.9. This nonstationary process quantifies the local turbulence decorrelation behavior. At longer time scales, R/S settles on an "asymptotic" power law in the "self-similarity range," over which $H=0.65$ and $H=0.74$ are determined from the R/S slope (shown by dashed lines) at the SOL and the LCFS area, respectively. The error bar of H is about 0.03, which is estimated from the statistical dispersion of the results from the eight calculated sub blocks of the data. Using SF method, the slope of the SF curve in the stationary range gives also H directly. In Figs. 4(c) and 4(f), we can see that the R/S and SF methods show good agreement for getting H, only with a slight difference for the low H case ($H=0.65$), in agreement with simulations.[25,26] In comparison with the SOL, the broader f^{-1} region and longer ACF tail at the LCFS zone are consistent with the higher Hurst parameter detected at that position. At $r=45.6$ cm inside the LCFS, the presence of

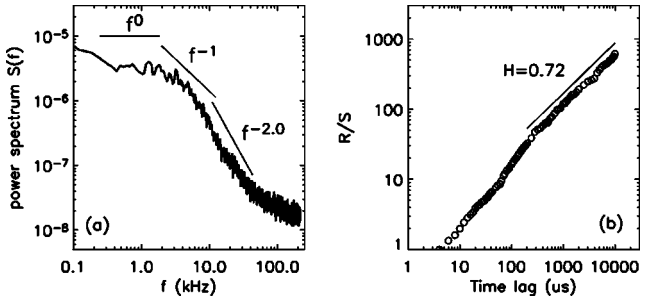

FIG. 5. (a) Power spectrum $S(f)$ and (b) R/S analysis of the density fluctuations measured at $r/a=1.04$ by thermal Li beams in an ohmic discharge (shot No. 61 028). The solid line in (b) shows the best fit to the slope of R/S ratio (open symbols) with $H=0.72$.

coherent modes perturbs the evaluation of the Hurst exponent. As CMs can correlate over long times with $H\approx 1.0$,[17] it is necessary to exclude their influence in the study of long-range dependence of the broadband turbulence. Such effects have been investigated in detail in Ref. 25 by adding a periodic sine function to a simulated fractional Gaussian signal in the R/S and SF analysis. It has been shown that the R/S scaling range affected by the CMs may cover the time range across the CM period because of the existence of a transition range inherent in the R/S algorithms, while for SF the effects of CMs on its scaling behavior is negligibly small for lags larger than the CM period. Similar phenomena also appear in our case. In Fig. 4(i), it can be clearly seen that the R/S curve has an increased slope around 100 μs, the main CM period. However, at time lags far above that, say $\geqslant$1500 μs marked by the vertical dotted line, the Hurst parameter of $H\approx 0.73$ can still be extracted from the straight part of R/S curve. On the other hand, the influence of CM on SF is much smaller and affects only the region up to the main CM period $\sim$100 μs. The upper part of the SF curve clearly scales as a power law with $H\approx 0.73$ (>0.5). Both the R/S and SF analysis suggest an existence of self-similarity of the background fluctuations at the plasma edge.

To search for the universality of SOC characteristics, we also extend our analysis to the density fluctuation data, which have been measured by two thermal Li beams in the SOL region.[33] The results show similar features to those obtained from the floating potential fluctuations. As an example, the power spectrum $S(f)$ and R/S values measured at a normalized radial location of $r/a=1.04$ in the SOL under similar ohmic discharge conditions are plotted in Fig. 5. In Fig. 5(a), $S(f)$ also exhibits three frequency regions with power-law indices of 0, -1, and -2, respectively. The corresponding R/S plot of Fig. 5(b) displays a self-similarity parameter $H\approx 0.72$ in the mesoscale time lags. In spite of some difference appeared in the $S(f)$ and R/S plots between the two type of fluctuation data, the common features, such as the presence of f^{-1} power-law dependence and Hurst parameter $H>0.5$, strongly support the idea that SOC is an important mechanism in plasma transport.

A further documentation of the turbulence in the edge of TEXTOR in the "nonshear" phase is given in Figs. 6 and 7. Figure 6 gives the radial profiles of Hurst parameter H and the local decorrelation time of turbulence τ_D, which are obtained from the R/S plot (open circles) and SF (solid triangles) and the e-folding time of ACF of the floating potential fluctuations, respectively for a large number of shots. Figure 6(b) shows that the τ_D values are slightly higher in the

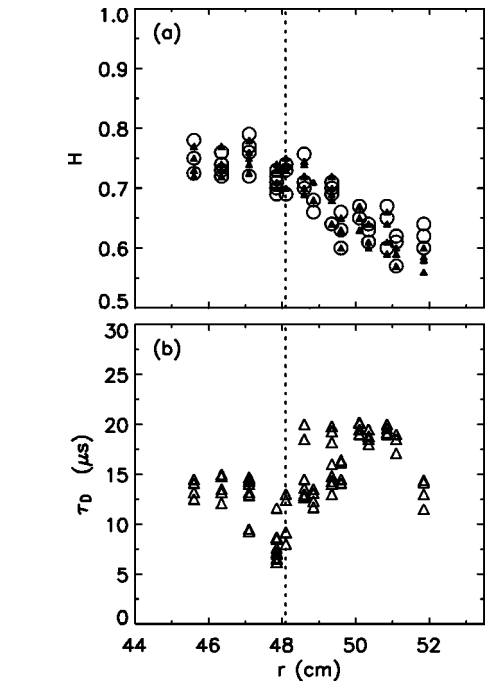

FIG. 6. The radial dependence of (a) Hurst parameter (H) estimated by R/S (open circles) and SF (small solid triangles) and (b) the local decorrelation time of turbulence (τ_D) in the nonshear discharge phase before biasing. The vertical dotted line marks the position of the last closed flux surface.

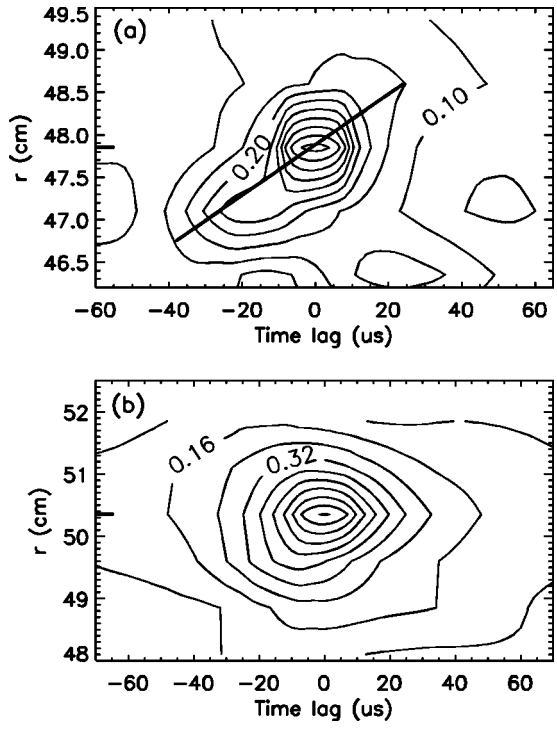

FIG. 7. Contours of the pairwise cross-correlation function (CCF) measured in (a) the plasma edge and (b) the scrape-off layer in the "nonshear" discharge phase before biasing. The motion of maximum CCF in (a) indicates a radially outward propagation in the plasma edge.

SOL than in the edge plasma region, implying that the local short time scale electrostatic fluctuations are more decorrelated in the edge plasma zone. The lowest τ_D values at the limiter location could be related to plasma diamagnetic drifts due to a sudden change of the pressure gradient at the last closed flux surface. In such a case, the decorrelation time of turbulence is dominated by the correlation length of the turbulence structures which are swept over the probe, but not by the temporal decay of the structure. Therefore, τ_D measured might be smaller than the real one.[31] In Fig. 6(a), it is seen that at all the detected radial locations, the Hurst parameters are well above 0.5, indicating the existence of long-range dependencies in the fluctuation dynamics in both the plasma edge and the SOL. Moreover, we find that the values of H in the "nonshear" plasma edge under the present conditions are appreciably higher than those in the SOL (other discharge conditions show different features, see Ref. 21). These results reveal a stronger avalanche transport behavior existing inside the LCFS.

In Fig. 7 we document the existence of long scale spatially correlated events. The measurements were performed using six radially spaced probes (7.5 mm separation between pins) and carried out in the plasma edge and in the SOL, respectively. The cross-correlation function (CCF) of the floating potential fluctuations between the six radial probes is then calculated. Shown in Figs. 7(a) and 7(b) are contours of the pairwise CCF of each probe with a reference one at $r=47.85$ cm in the plasma edge and $r=50.35$ cm in the SOL, respectively. In Fig. 7(a), the motion of the position of maximum CCF to larger time lags indicates an outward propagation in the plasma edge at an effective speed of $V_r \approx 330$ m/s. To have a good identification of a pure SOC-type avalanche propagating behavior, the CM harmonic frequency components detected at several inner plasma edge locations have been filtered from the fluctuation data prior to calculating the CCFs. This motion in the radial direction clearly identifies this feature as an avalanche. This result is similar to that observed in DIII-D of the temperature fluctuations.[14] Note that the radial extent of the coherent feature is ~ 22 mm, much larger than the local gyroradius ($\rho_i \approx 0.4$ mm), which is the typical scale length for gyro-Bohm scaling.[1] On the other hand, in the SOL, no clear signature of radial propagation is manifested in the measured CCFs, as seen in Fig. 7(b). The results appear to be in accordance with lower H values detected in the SOL [see Fig. 6(a)], where less avalanche behavior is expected.

To summarize, in the "nonshear" discharge phase of TEXTOR, experimental results of the power spectra, autocorrelation (cross-correlation) functions and self-similarity parameters calculated from both the potential and density fluctuations all show some characteristic properties of SOC, i.e., existence of f^{-1} falloff in the power spectrum, long-range time dependencies showing by slowly decaying tail in ACF, large scale spatial correlations and avalanche like events by CCF, and self-similar character of fluctuations by R/S and SF analysis of Hurst parameters well larger than 0.5. All these facts are consistent with plasma transport characterized by SOC dynamics.

B. Change of long-range dependence and local turbulent correlation by a sheared edge $E_r \times B$ flow in the "shear" phase

The influence of a sheared $E_r \times B$ flow on long-term and short-term correlations can most conveniently be studied in biasing experiments. Up to now, the predictions of shear flow effects on long-range time correlations are mainly based on the sandpile modeling, in which the R/S analysis indicates a decorrelation (i.e., decrease of correlation) of avalanches when a sheared wind flow is included into the sandpile.[8] Experimental investigation on this aspect is very limited. In Ref. 11, evidence has been shown that the H values near the edge shear flow layer in Wendelstein 7 Advanced Stellarator are slightly lower than those on either side, in agreement with the sandpile modeling. The interpretation of data measured in regions where the poloidal plasma flow $V_\theta \neq 0$ deserves special attention. As pointed out by several authors,[29,31] the presence of a plasma rotation may significantly modify the structure of frequency spectrum and also the correlation time of fluctuations depending on whether they are measured in the moving frame or the laboratory rest frame. The reason is that a poloidal flow can affect $S(f)$ by Doppler shift in frequencies and ACF due to the movement of the correlation structures across the probe. From Fig. 2(b), we can see that in our experiment the large poloidal flows during the biasing phase are mainly located within $r \approx 46.7$ to 48.3 cm, since V_θ is dominated by the E_r/B effects (B is magnetic field) as substantiated by direct measurements.[34] To mitigate the flow impact, the frequency spectra measured in this region have been reconstructed following the method used in Ref. 29. The correction of Doppler shift in $S(f)$ is made by formula $f=\hat{f}-\overline{k_\theta}(f)V_\theta/2\pi$, where $\hat{f}$ and f are the frequency measured in the laboratory frame and the plasma rest frame, respectively, and $\overline{k_\theta}(f)$ is the averaged poloidal wave number at a given frequency f. Here, $\overline{k_\theta}(f)$ data are taken from previous measurements by a fixed two-point probe with an average value about $1-2$ cm^{-1}.[35] The ACFs and R/S (and SF) values in those locations are then calculated in a reconstructed time domain, which is reverse transformed from the corrected frequency domain. An example of such a correction at the location of $r=48.1$ cm is shown in Fig. 8, where the $S(f)$, ACF, and R/S ratios before (black color) and after (red color) the correction are compared. From Fig. 8(a), it is seen that either before or after the correction, the shape of $S(f)$ in the biasing phase can be characterized by two parts, one roughly following f^{-1} decay in the low-frequency range and the other keeping flat at high-frequency region. Although Doppler shift modifies the structure of $S(f)$ in the frequency domain, these leading features of $S(f)$ remain unchanged. The modifications on ACF and R/S ratio due to Doppler shift are shown in Figs. 8(b) and 8(c), where τ_D decreases slightly and H value is reduced from 0.87 to 0.85 after the correction. It must be pointed out that such corrections can only minimize the flow effects, but may not be fully accurate, as no direct and simultaneous measurements of V_θ and $\overline{k_\theta}(f)$ were available.

The radial dependencies of H and τ_D before (black symbols) and during (red symbols) the biasing phase are plotted

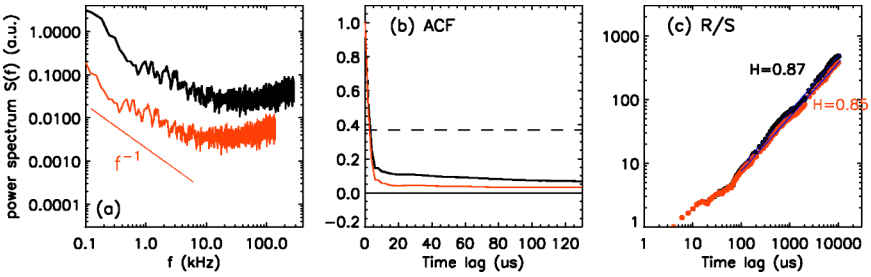

FIG. 8. (Color online). Comparison of (a) frequency spectrum $S(f)$, (b) autocorrelation function (ACF), and (c) R/S ratio of floating potential fluctuations detected at $r=48.1$ cm during biasing phase without (black curves and symbols) and with (red curves and symbols) the correction due to Doppler shift in frequency domain. Note that $S(f)$ shown in (a) is in arbitrary unit.

in Figs. 9(a) and 9(b). Note that in Fig. 9(a), the H values calculated from R/S (open circles) and SF (solid triangles) during the biasing phase are both plotted to validate their accuracy. For comparison, Figs. 9(c) and 9(d) show the radial profiles of the fluctuation amplitudes and the edge electric field E_r shear measured in a number of shots under the same discharge conditions before and during the biasing. Figure 9(a) clearly indicates that during the biasing phase the H values are increased in the SOL and in the region of negative E_r shear, as is seen in Fig. 9(d). Details of $S(f)$, ACF, and R/S ratio before/during the biasing have been plotted in Fig. 10 for two radial positions, i.e., one outside flow-shear region at $r=50.1$ cm and the other at the location of maximum flow-shear at $r=48.1$ cm in the biasing phase. At the first position, Fig. 10(a) shows that during biasing, the shape of $S(f)$ is changed considerably and the range of f^{-1} power falloff becomes much more broader, suggesting that the interactions among the avalanches are much stronger than before or that diffusion is now much less important, according to the modeling in Ref. 10. Correspondingly, in the biasing phase, the tail of ACF becomes longer and thus the Hurst parameter is higher than before over the self-similarity range, as seen in Figs. 10(b) and 10(c). At the second position where there is a velocity shear during the biasing, the $S(f)$ structure is also clearly modified with respect to before [see Fig. 10(d)]. At the high-frequency region ($f \geqslant 10$ kHz), $S(f)$ becomes flat; however, in the low-frequency end, $S(f)$ assumes a more f^{-1} like power-law dependence in the frequency region of $0.1 \sim 10$ kHz. Because of this, the ACF tail [see Fig. 10(e)] turns to be more flat in the biasing phase and hence the H value [see Fig. 10(f)] is increased from 0.74 before to 0.85 during the biasing. Indications are that with biasing the importance of long-range dependence in the flow shear region is increased and that the radial propagation of avalanches leads to an increase of self-similarity in fluctuations at the SOL.

It should be noted, however, that the subsistence of long-range correlations in the flow shear region is surprising, and in contrast with the sandpile simulations.[8] Several factors might be thought of as possibly able to contaminate the H values. (i) On Alcator-C-Mod tokamak[36] contamination by low-frequency perturbations at 50–60 Hz has been found to increase the H values. In our case, no such perturbations either clearly show up in time traces of the raw signals [except for 25 Hz ringing of power supply as can be seen in Fig. 1(b) in the biasing voltage signal, which has been filtered on the fluctuation data analyzed, as stated earlier] nor in the stationarity tests of the fluctuation data during the biasing

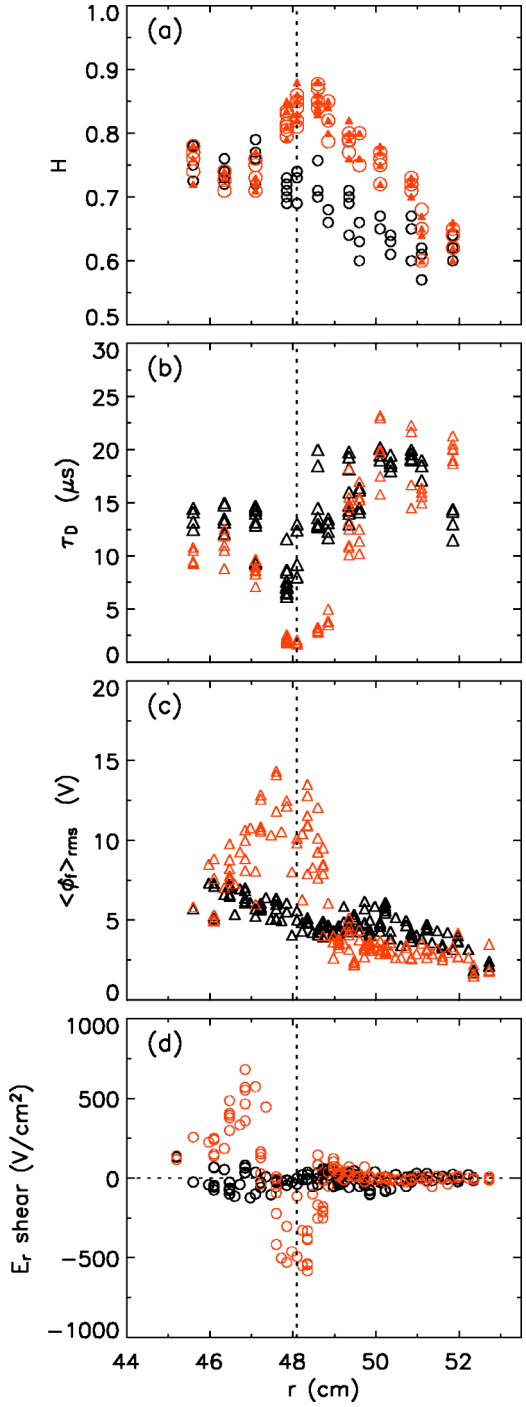

FIG. 9. (Color online). Radial profiles of (a) Hurst parameter (H) estimated by R/S (open circles) and SF (small solid triangles), (b) local decorrelation time of turbulence (τ_D), (c) fluctuation amplitude, and (d) radial electric field E_r shear before (black symbols) and during (red symbols) the biasing phase. The vertical dotted line marks the position of the last closed flux surface.

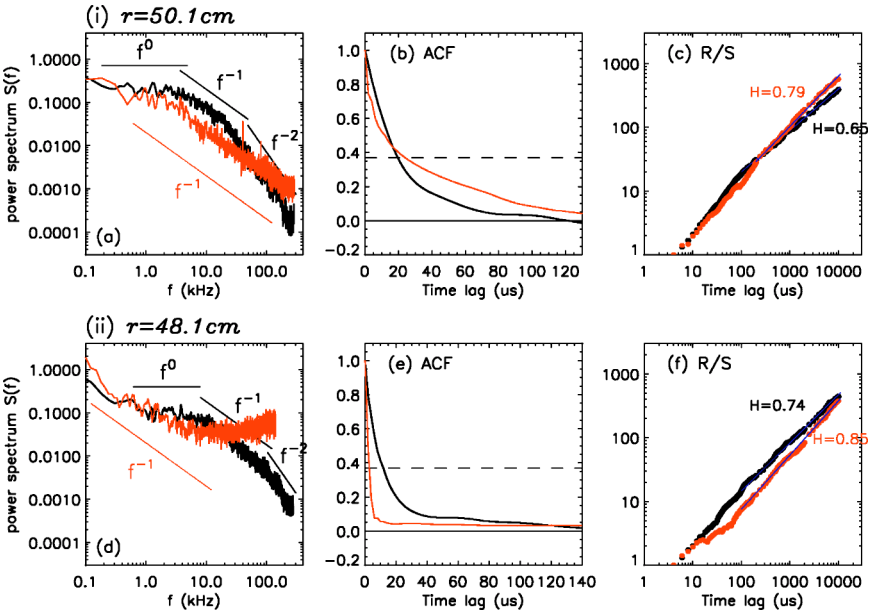

FIG. 10. (Color online). Comparison of power spectrum $S(f)$, autocorrelation function (ACF), and R/S ratio before (black curves and symbols) and during (red curves and symbols) the biasing at two radial locations: (i) $r=50.1$ cm outside the flow-shear region and (ii) $r=48.1$ cm where the flow-shear is maximum.

phase. (ii) The accurateness of Doppler-shift correction could also affect H value in the high-flow zone ($46.7\ \text{cm} < r < 48.3\ \text{cm}$). However, in the outer SOL region ($r > 49$ cm) the flow is very small or close to zero and this correction cannot therefore play a role. One plausible explanation for the deviation with respect to the sandpile simulation may come from the modeling done in Ref. 10, where the interplay between the diffusive and SOC transport dynamics is studied. For the dominant discontinuous SOC transport channel and the subdominant continuous diffusive channel, the modeling indicates that with the increase of diffusivity ratio, the $1/f$ region of the power spectrum shrinks and the Hurst exponent decreases as the continuous smoothing of the local inhomogeneities in the slope profile by the increased diffusion makes avalanches more difficult to take place. In contrast, at low ratio of diffusivity, the diffusive component cannot well balance the source at the submarginal level, causing the slope to buildup so that large SOC-type avalanches can occur. This seems to be consistent with our experiment. In the shear phase, the local turbulence is strongly decorrelated, which will be further elucidated in the next paragraph, and thus the SOC channel prevails. The present results demonstrate that an $E_r \times B$ flow shear alone, at least in our case, is not sufficient to suppress avalanchelike transport. The question as to the conditions necessary to effectively decorrelate SOC-type avalanches by sheared flow appears therefore still unanswered. The fact that the Hurst parameters are almost unchanged during the biasing phase in the positive E_r shear locations, as seen in Fig. 9(a), remains also to be explained.

On the other hand, the role of an $E_r \times B$ flow shear on the decorrelation of local turbulence is clearly shown in our experiment. Comparing Figs. 9(b) and 9(d), it can be seen that the local decorrelation time τ_D, drops sharply in the negative and slightly in the positive E_r shear region in the biasing phase. This result is consistent with other experimental data[31,35] and also with theoretical predictions.[37] In the BDT model of Ref. 37, it is described that fluid elements can be fissured by a poloidal velocity shear in addition to their radial scattering. As a consequence, the local turbulent eddy can be strongly decorrelated in the case of shear flow. According to the model, the shear decorrelation time τ_s is defined as the time in which the correlation volume is separated poloidally by a correlation length $\ell_{c\theta}$, i.e., $\tau_s \approx \ell_{c\theta} \ell_{cr}^{-1} |E_r'/B|^{-1}$, where ℓ_{cr} denotes the radial correlation length and $E_r' = \partial E_r / \partial r$ is the radial electric field shear. In the case of strong shear $\tau_s \ll \tau_c$, where τ_c is the characteristic time of the diffusive scattering of the ambient turbulence, the fluctuations are effectively decorrelated at a time $\tau_{sc} \approx \tau_s^{2/3} \tau_c^{1/3}$. For a comparison with the measurements of τ_D, we calculated the local τ_{sc} value using the measured parameters around the LCFS, where $E_r' \approx 500\ \text{V/cm}^2$ [see Fig. 9(d)] and $B \approx 2.3$ T. Taking $\tau_c \approx 10\ \mu$s in the "nonshear" phase when V_θ is about zero [see Fig. 9(b)] and assuming $\ell_{c\theta} \approx \ell_{cr}$, gives $\tau_{sc} \approx 1.3\ \mu$s. This value is very close to the measured decorrelation time of $\sim 2\ \mu$s in the biasing phase in the vicinity of the LCFS, as seen the Fig. 9(b). These results indicate that the influence of negative $E_r \times B$ shear on the decorrelation of local turbulence is still valid. Further evidence for the shear effect on short time events can also be seen from Figs. 10(d)–10(f), where $S(f)$ is flattened (randomized like white noise) at the high-frequency range, R/S slope (H value) is close to 0.5 in the small time lags and accordingly τ_D is reduced remarkably in the ACF. From Fig. 9 it is seen that the reduction of τ_D in the positive E_r shear region is much less pronounced.

IV. SUMMARY

In conclusion, the floating potential fluctuation data measured at the plasma edge and the SOL of TEXTOR in the edge biasing experiments, together with the density fluctuation data detected in the SOL of ohmic discharges on TEXTOR, have been analyzed for the study of SOC-relevant phenomena. Evidence has been found that, in "nonshear" discharge phase before biasing, the fluctuations exhibit f^{-1}

power-law dependence in their spectra, the autocorrelation function displays long decaying tail, the R/S and SF analysis show self-similarity parameters well larger than 0.5 at all measured locations and a radial propagation of avalanche events is manifested in the edge plasma area. All these results are consistent with the presence of a transport channel showing SOC behavior and plasma transport mechanisms based on avalanches.

During the biasing phase of the edge electrode polarization experiment, with the generation of an edge radial electric field E_r and therefore an edge $E_r \times B$ velocity shear, the Hurst exponents are enhanced substantially in the negative E_r shear zone and also in the SOL. The results indicate that an $E_r \times B$ flow shear alone, at least in our case, is not sufficient to suppress the SOC-type transport. $E_r \times B$ velocity shear, especially in the negative E_r shear region, can however very well decorrelate the local turbulence by reducing the local decorrelation time close to theoretically predicted values. The diffusive transport channel is thereby very strongly suppressed. We tend to conclude that (i) in the ohmic phase most transport is diffusive in the TEXTOR edge, while, with strong shear, SOC transport prevails, and (ii) in the negative E_r shear region, "*the dynamics governing the decorrelation of the local fluctuations and the long-range time dependencies are probably different, one being the decorrelation of the turbulence and the other being the decorrelation of the transport events (avalanches)*" as stated in Ref. 11.

ACKNOWLEDGMENTS

This work was partially supported by the Alexander von Humboldt foundation. The authors would like to thank the support from the TEXTOR team.

APPENDIX: FREQUENCY SPECTRA, AUTOCORRELATION FUNCTIONS, AND HURST EXPONENTS

The shape of the auto-power frequency spectrum $S(f)$ which is the Fourier transform of the autocorrelation function, is closely linked to the correlation properties of a signal. For instance, for a sine periodic wave, the $S(f)$ has a narrow band peak indicating that all fluctuations occur at the same frequency, while for a white noise the $S(f)$ is nearly flat implying that the fluctuation intensity does not depend on any preferable frequency. According to the work of Hwa and Kadar on SOC dynamics in models of "running sandpile," the shape of $S(f)$ can be divided into three distinct frequency regions, each with characteristic power dependence[5,30] and discussed in our main text under Sec. III A. For a long time, the existence of an asymptotic power falloff of $S(f)$ at the high-frequency range with decay indices close to -2 or higher has been observed.[27] Also at the lowest-frequency part, S(f) exhibits a weak dependence of frequency. Because of a possible connection to the paradigm of SOC, the interacting avalanche subrange has captured much attention in recent years in the search for the f^{-1} power law in the intermediate frequency domain.[12,14,17,28,29]

Another expected property of SOC-governed systems is the existence of long-range dependence or self-similarity in the fluctuation data. In general, self-similarity of a time series is linked to an algebraic tail (i.e., slowly decaying for long time lags) in the autocorrelation function (ACF).[32] The related concepts can be seen as follows: For studying the correlation structure of a time series, $X \equiv \{X_t : t=1,2,\ldots n\}$, on different time scales, a standard method is to divide X into subseries of lengths $m=2^k$ data points, where $k=0,1,2,\ldots M$, and $2^M \ll n$. For each m, the values of the data points in each subseries are averaged to generate a new coarse-grained time series, $X^{(m)} \equiv \{X_u^{(m)} : u=1,2,\ldots,n/m\}$, where $X_u^{(m)} = (X_{um-m+1} + \cdots + X_{um})/m$. The corresponding variance σ_m^2 can be written as:

$$\sigma_m^2 = \frac{\sigma^2}{m} + \frac{2\sigma^2}{m^2} \sum_{p=1}^{m} \sum_{\tau=1}^{p-1} \rho(\tau) \approx \frac{\sigma^2}{m} \left[1 + 2 \sum_{\tau=1}^{m-1} \rho(\tau) \right], \qquad (1)$$

where σ^2 denotes the variance of the original time series, X, $\rho(\tau) = \mathrm{cov}\{X_i, X_{i+\tau}\}/\sigma^2$ denotes the ACF of X, and τ is the time lag. For a random variable X, which corresponds to Gaussian processes with short-range time dependence, σ_m^2varies asymptotically as m^{-1} when $m \to \infty$. However, if the integral term in Eq. (1) diverges, we rather find σ_m^2 decreases slower than m^{-1} and the asymptotic dependence becomes $\sigma_m^2 \sim m^{-\beta} (0 < \beta < 1)$ as $m \to \infty$. This can be further written as $\lim_{m\to\infty} \sigma_m^2 \propto m^{-\beta} = m^{2H-2}$, where $H = 1 - \beta/2$ is introduced as *Hurst parameter* $(0.5 < H < 1)$. In such a case, the ACF of X decays as a power law, i.e., $\rho(\tau) = \delta^2(\tau^{2-\beta})/2 \propto \tau^{-\beta}$, where the operator δ^2 denotes the second-order central derivative operator in finite differences. As a consequence, it is said that X exhibits *long-range dependence*.

Although the calculation of ACF can provide direct information on the long-range time dependence, it is not easy to accurately determine the values of β and H via its long time lag tail, for which very high statistics are needed. However, there are some techniques effective for the determination of long-range dependence in a finite time series. One such technique is the rescaled range (R/S) analysis proposed by Mandelbrot and Willis, following the pioneering work of Hurst on the hydrological analysis.[22] For a time series of length, $X \equiv \{X_t : t=1,2,\ldots n\}$, with mean $\overline{X}(n)$ and standard deviation $S(n) = \sqrt{\sigma^2(n)}$, the R/S ratio is defined as

$$\frac{R(n)}{S(n)} = \frac{\max(0, W_1, W_2, \ldots W_n) - \min(0, W_1, W_2 \ldots W_n)}{\sqrt{\sigma^2(n)}}, \qquad (2)$$

where $W_k = \Sigma_{i=1}^{k} X_i - k\overline{X}(n)$. Then the expected value of R/S depends asymptotically on n as $n \to \infty$, i.e.,

$$E\{R(n)S(n)\} \underset{n\to\infty}{\to} cn^H,$$

where the Hurst exponent H, expresses increasing long-range dependence as H increases from $1/2$ to 1; namely, $H = 1/2$ for a random process and $H > 1/2$ for a sequence with long-term correlations. It has been shown that, in comparison to the direct calculation of the ACF or other altemative methods calculating H, the R/S analysis is remarkably robust.[23]

Aside from R/S, another robust technique for determining H is via structure functions (SFs).[24] The SF method has been recently discussed in detail by Yu *et al.*[25] with several advantages, including straightforward tests for stationarity of data samples and reduced sensitivity to coherent mode effects, etc. For a process (or time series), $X \equiv \{X_t : t = 1, 2, \ldots, n\}$, the qth-order structure function, $S_{x,q}(\tau)$, is defined as the qth moment of the increments of $X(t)$,

$$S_{x,q}(\tau) \equiv \langle |X(t_i + \tau) - X(t_i)|^q \rangle, \tag{3}$$

where i denotes the ith data point, τ is the time lag, and $\langle\rangle$ denotes the ensemble average. If $X(t)$ is self-similar over a certain range of τ, $S_{x,q}(\tau)$ in this range is thus scaled as

$$S_{x,q}(\tau) = c_q \tau^{qH(q)}, \tag{4}$$

where c_q is approximately constant and $H(q)$ is the Hurst exponent. The SF method is applicable to either nonstationary processes with stationary increments such as fractional Brownian motion or cumulative sums of stationary self-similar processes such as fractional Gaussian noise. In the latter case, $S_{x,q}(\tau)$ in Eq. (4) exhibits no scaling with τ, i.e., $qH(q) \equiv 0$, then the original data series $X(t)$ in Eq. (3) is replaced by its cumulative one, $W_k = \Sigma_{i=1}^{k} X_i$, therefore, Eq. (3) becomes

$$S_{W,q}(\tau) \equiv \langle |W(t_i + \tau) - W(t_i)|^q \rangle. \tag{5}$$

Then, the Hurst exponent H can be determined from Eq. (4) using $S_{w,q}(\tau)$ instead of $S_{x,q}(\tau)$.

[1] B. B. Kadomtsev, *Plasma Turbulence* (Academic, London, 1965).
[2] R. J. Fonck, N. Bretz, G. Cosby *et al.*, Plasma Phys. Controlled Fusion **34**, 1993 (1992).
[3] F. W. Perkins, C. W. Barnes, D. W. Johnson *et al.*, Phys. Fluids B **5**, 477 (1993).
[4] P. H. Diamond and T. S. Hahm, Phys. Plasmas **2**, 3640 (1995).
[5] D. E. Newman, B. A. Carreras, P. H. Diamond, and T. S. Hahm, Phys. Plasmas **3**, 1858 (1996).
[6] X. Garbet and R. E. Waltz, Phys. Plasmas **5**, 2836 (1998).
[7] P. Bak, C. Tang, and K. Wiesenfeld, Phys. Rev. Lett. **59**, 381 (1987).
[8] D. E. Newman, B. A. Carreras, and P. H. Diamond, Phys. Lett. A **218**, 58 (1996).
[9] B. A. Carreras, D. E. Newman, V. E. Lynch, and P. H. Diamond, Phys. Plasmas **3**, 2903 (1996).
[10] R. Sánchez, D. E. Newman, and B. A. Carreras, Nucl. Fusion **41**, 247 (2001).
[11] B. A. Carreras, B. Ph. van Milligen, M. A. Pedrosa *et al.*, Phys. Rev. Lett. **80**, 4438 (1998).
[12] M. A. Pedrosa, C. Hidalgo, B. A. Carreras *et al.*, Phys. Rev. Lett. **82**, 3621 (1999).
[13] G. Y. Antar, S. I. Krasheninnikov, P. Devynck *et al.*, Phys. Rev. Lett. **87**, 065001 (2001).
[14] P. A. Politzer, Phys. Rev. Lett. **84**, 1192 (2000).
[15] R. Sánchez, B. Ph. van Milligen, D. E. Newman, and B. A. Carreras, Phys. Rev. Lett. **90**, 185005 (2003).
[16] J. A. Krommes and M. Ottaviani, Phys. Plasmas **6**, 3731 (1999).
[17] B. A. Carreras, B. Ph. van Milligen, M. A. Pedrosa *et al.*, Phys. Plasmas **5**, 3632 (1998).
[18] R. Jha, P. K. Kaw, D. R. Kulkarni, J. C. Parikh, and ADITYA Team, Phys. Plasmas **10**, 699 (2003).
[19] R. R. Weynants, G. V. Oost, G. Bertschinger *et al.*, Nucl. Fusion **32**, 837 (1992).
[20] S. Jachmich, G. V. Oost, R. R. Weynants *et al.*, Plasma Phys. Controlled Fusion **40**, 1105 (1998).
[21] Y. Xu, S. Jachmich, and R. R. Waynants, Czech. J. Phys. **53**, 869 (2003).
[22] H. Hurst, Trans. Am. Soc. Civ. Eng. **116**, 770 (1951); B. B. Mandelbrot and J. R. Wallis, Water Resour. Res. **4**, 909 (1968).
[23] B. B. Mandelbrot and J. R. Wallis, Water Resour. Res. **5**, 967 (1969).
[24] A. Davis, A. Marshak, W. Wiscombe, and R. Cahalan, J. Geophys. Res. **99**, 8055 (1994).
[25] C. X. Yu, M. Gilmore, W. A. Peebles, and T. L. Rhodes, Phys. Plasmas **10**, 2772 (2003).
[26] M. Gilmore, C. X. Yu, T. L. Rhodes, and W. A. Peebles, Phys. Plasmas **9**, 1312 (2002).
[27] S. J. Levinson, J. M. Beall, E. J. Powers *et al.*, Nucl. Fusion **24**, 527 (1984).
[28] T. L. Rhodes, R. A. Moyer, R. Groebner *et al.*, Phys. Lett. A **253**, 181 (1999).
[29] B. A. Carreras, R. Balbin, B. Ph. van Milligen *et al.*, Phys. Plasmas **6**, 4615 (1999).
[30] T. Hwa and M. Kadar, Phys. Rev. A **45**, 7002 (1992).
[31] C. P. Ritz, H. Lin, T. L. Rhodes, and A. J. Wootton, Phys. Rev. Lett. **65**, 2543 (1990).
[32] J. Beran, *Statistics for Long-Memory Processes* (Chapman and Hall, New York, 1994).
[33] A. Huber, A. V. Nedospasov, U. Samm, and B. Schweer, J. Nucl. Mater. **266**, 546 (1999).
[34] H. Van Goubergen, S. Jachmich, G. V. Oost *et al.*, *Proceedings of 26th EPS Conference on Controlled Fusion and Plasma Physics*, Masstricht (European Physical Society, Petit-Lancy, 1999), Vol. 23J, p. 1049.
[35] J. Boedo, D. Gray, S. Jachmich *et al.*, Nucl. Fusion **40**, 1397 (2000).
[36] Anonymous referee (private communication).
[37] H. Biglari, P. H. Diamond, and P. W. Terry, Phys. Fluids B **2**, 1 (1990).